

Article

Control of Cell Adhesion and Growth on Polysaccharide-Based Multilayer Coatings by Incorporation of Graphene Oxide

Tonya Andreeva ^{1,2,*} , Alexander Rudt ¹, László Fábrián ³, Ferhan Ayaydin ^{4,5}, Ivan Iliev ⁶ , Ole Jung ⁷, Mike Barbeck ⁷ , Andras Dér ³ , Rumen Krastev ¹  and Stefka G. Taneva ² 

¹ Faculty of Life Sciences, Reutlingen University, 72762 Reutlingen, Germany

² Institute of Biophysics and Biomedical Engineering, Bulgarian Academy of Sciences, 1113 Sofia, Bulgaria

³ Institute of Biophysics, HUN-REN Biological Research Centre, H-6701 Szeged, Hungary

⁴ Functional Cell Biology and Immunology Advanced Core Facility (FCBI), Hungarian Centre of Excellence for Molecular Medicine (HCEMM), University of Szeged, H-6720 Szeged, Hungary

⁵ Cellular Imaging Laboratory, HUN-REN Biological Research Centre, H-6726 Szeged, Hungary

⁶ Institute of Experimental Morphology, Pathology and Anthropology with Museum, Bulgarian Academy of Sciences, 1113 Sofia, Bulgaria; taparsky@abv.bg

⁷ Clinic and Polyclinic for Dermatology and Venereology, University Medical center Rostock, 18057 Rostock, Germany

* Correspondence: tonya.andreeva@reutlingen-university.de; Tel.: +49-(0)7121-271-2043

Abstract: Controlling cell adhesion, viability, and proliferation on solid surfaces is critical for the successful implantation and proper functioning of temporary and permanent medical devices. While, with temporary or removable implants as well as surgical instruments, even slight cellular adhesion leads to an increased risk of secondary infections, bleeding and other complications, good cellular adhesion and viability are essential for the rapid healing and successful integration of permanent implants. This work was motivated by the growing interest in the construction of biocompatible and biodegradable coatings for the biofunctionalization of medical devices. Polysaccharide-based coatings are well known for their biocompatibility, but they are non-cell-adhesive, which hinders their application as implant coatings. In this study, we demonstrate that the incorporation of one or more graphene oxide layers in hyaluronic acid/chitosan multilayers is one avenue to regulate the degree of unspecific adhesion and growth of different cells (human umbilical vein endothelial cells, HUVEC, and mouse embryonic fibroblasts, 3T3). Furthermore, we demonstrate that this approach allows cell adhesion to be regulated across the entire range between completely prevented and highly promoted cell adhesion without introducing systemic cytotoxicity. These findings may contribute to the establishment of a new approach to adapt medical devices to cells and tissues.

Keywords: polyelectrolyte multilayers; graphene oxide; biocompatible coatings; cell adhesion; composite biomaterials



Citation: Andreeva, T.; Rudt, A.; Fábrián, L.; Ayaydin, F.; Iliev, I.; Jung, O.; Barbeck, M.; Dér, A.; Krastev, R.; Taneva, S.G. Control of Cell Adhesion and Growth on Polysaccharide-Based Multilayer Coatings by Incorporation of Graphene Oxide. *Coatings* **2024**, *14*, 570. <https://doi.org/10.3390/coatings14050570>

Academic Editor: Alina Vladescu

Received: 12 April 2024

Revised: 26 April 2024

Accepted: 30 April 2024

Published: 5 May 2024



Copyright: © 2024 by the authors. Licensee MDPI, Basel, Switzerland. This article is an open access article distributed under the terms and conditions of the Creative Commons Attribution (CC BY) license (<https://creativecommons.org/licenses/by/4.0/>).

1. Introduction

Implant materials (mostly metals, ceramics, plastics, and textiles, as well as combinations of them) are primarily selected for specific applications based on their mechanical, anti-corrosive, and load bearing properties. In order to control the human body reactions to the implant materials, they are biofunctionalized by surface modifications. Among a large number of possible surface modifications, polymer coatings, and particularly polyelectrolyte multilayer (PEM) coatings have the great advantage of being able to mask the surface of the underlying base material, owing to their specific properties, without affecting the bulk material qualities [1]. Although they are less than 100 nm thin, PEMs endow the surface with specific surface characteristics, including roughness [2,3], topography [4,5], stiffness [6–8], surface charge [9,10], wettability [10], surface energy [11], etc., which have been shown to be essential for complex phenomena such as protein adsorption and cell adhesion. All those properties affect one or more aspects of cell behavior in

terms of morphology, adhesion, proliferation, migration, differentiation, gene expression, and metabolism.

The assembly of the PEM coatings, their surface and bulk properties are strongly dependent on the choice of polyelectrolytes (PEs), their concentration and molecular weight, the mechanism of PEM assembly, and the deposition parameters, such as pH, ionic strength, and temperature [12–14]. Cell adhesion and viability are strongly influenced by the mechanical properties and hydration of PEM coatings, the adhesion being promoted by higher rigidity and lower hydration [6,15].

Polyelectrolyte multilayers made from hyaluronic acid (HA) and chitosan (Ch) are considered biocompatible [16]. These PEMs have been used in various biomedical applications, such as wound healing [17], drug delivery [18], and tissue engineering [19–21], owing to their biocompatibility, biodegradability [22], and resistance to bacterial adhesion [23–25]. Studies have shown that HA/Ch multilayers are resistant to protein adsorption [26,27], do not elicit an immune response [28], and do not cause cytotoxicity or genotoxicity [14].

However, the fact that HA/Ch multilayers do not support the adhesion and spreading of fibroblasts [28] and chondrosarcoma cells [22] could be a drawback limiting their application in the field of medical devices. Since the anti-adhesive behavior of HA/Ch films is attributed to their considerable hydration, as well as relatively high softness and elasticity [22], two possible approaches to enhance the cell adhesion and spreading were so far employed. The first one is based on the post-assembling chemical cross-linking of the multilayers in the presence of a water soluble 1-ethyl-3-(3-dimethylamino-propyl)carbodiimide (EDC) in combination with N-hydroxysulfosuccinimide (sulfo-NHS) [29]. Although chemical crosslinking increased the PEM film's stiffness drastically (tenfold), thus favoring cell adhesion and spreading [30], it reduced the degradability of HA/Ch coatings [28,29] and their usability as drug-delivery systems. Moreover, EDC, like other chemical crosslinkers, was proven to induce interchain cross-linking within double-stranded DNA and, finally, cell death [31]. The second approach actively applied for modification of the mechanical properties of PEM and hydrogels, as well as enhancement of cell adhesion, was based on the incorporation of other polymeric or non-polymeric components, like gold nanoparticles [32], bioactive glass nanoparticles [33], graphene oxide (GO) sheets [34], and many other colloids [35].

Numerous studies have proven that GO is not only non-toxic to cells but also improves mammalian cell attachment, growth, and proliferation on different materials, therefore has very good cell- and bio-compatibility [36]. In a comprehensive study, three different cell lines with a broad range of characteristics were grown on a free-standing reduced GO paper, namely Vero cells (African green monkey kidney cells which are robust and have a high propensity for growth and proliferation), embryonic bovine cells (with a limited lifespan resembling the cells *in vivo*), and Crandell-Rees feline kidney cells (finicky, delicate cells with a relatively low growth rate and proliferation); all revealed consistent cell growth and proliferation with cells retaining their native shape and forming a confluent monolayer as observed in the live–dead test [37]. But as for the mechanism by which GO regulates the degree of adhesion and growth of different cells, there is still much room for investigation. Surface topology and roughness are contributing factors to cell accommodation at the surface, and GO sheets create topographies with nanoscale roughness that supports cell attachment [38]. Protein adsorption on a material surface is also crucial for the biocompatibility of biomaterials, and increasing evidence has shown that cells recognize and interact with the adsorbed proteins and respond to their amount and conformation by changes in adhesion, migration, proliferation, and differentiation [39]. GO interacts strongly with proteins due to its negative charge and reactive functional groups [40] and thus enhances cell accommodation at the surface.

Our recent studies have shown that the physicochemical properties, surface heterogeneity, and growth mechanism of composite GO/PEM assemblies depend on both the charge of the PE couples and the number and localization of GO layers in the polymer matrix [41]. We also found that the extent of albumin adsorption and platelet adhesion to composite HA/Ch/GO films could be broadly adjusted by varying the number and localization of the GO layers in the polymer matrix [38]. So, inspired by these capabilities of composite HA/Ch/GO coatings, in this study, we investigated the possibility of enhancing and controlling the adhesion and growth of two essential cell types (human umbilical vein endothelial cells (HUVECs) and 3T3 mouse fibroblast cells) by incorporating one or more GO layers at different positions in natural HA/Ch polyelectrolyte matrices.

2. Materials and Methods

2.1. Build-Up of PEM Coatings

Polyethyleneimine (PEI) (MW \approx 750 kDa, 50 wt.% solution, Sigma Aldrich, Steinheim, Germany), chitosan (Ch) (MW \approx 50–190 kDa, 75–85% deacetylated, Sigma Aldrich, Steinheim, Germany), hyaluronic acid (HA) (MW \approx 360 kDa, Lifecore Biomedical, LLC, Chaska, MN, USA), and graphene oxide water dispersion (4 mg/mL, from Graphenea, Spain) were used as received.

Depending on the research envisaged, PEM films were prepared either on silicon (100) wafers (10 \times 10 mm, CrysTec GmbH, Berlin, Germany), preliminarily cleaned by consecutive ultrasonication in acetone and isopropanol (2 min each); on glass coverslips (Carl Roth GmbH, Karlsruhe, Germany), cleaned successively in hot (60 °C) solutions of 2% Mucosol, 10 mM SDS and 0.1 M HCl (all from Sigma-Aldrich); or on 24-well plates (Corning Inc., New York, NY, USA). All PEMs were constructed by layer-by-layer (LbL) deposition with the application of the dip coating technique. PEI was dissolved in ultrapure water to a concentration of 2 mg/mL (pH 7.0) and deposited for 10 min as the first layer, acting as a uniform anchoring network for the formation of consecutive layers. Then, the PEM films were constructed by the alternative deposition of HA and Ch (10 min each), both dissolved in 250 mM NaCl to a concentration of 1 mg/mL (pH 5.5), followed by three washing steps (2 min each) in 250 mM NaCl (pH 5.5). GO dispersion was diluted with ultrapure water to a concentration of 0.5 mg/mL and ultrasonicated (50 Hz, Isolab, Germany) for 1 min prior to use. For the deposition of GO layers, the substrates were kept in contact with the GO suspension for 10 min, followed by three washing steps in water (2 min each). After the last deposition step, the samples were washed with water and dried in a nitrogen stream. Each experiment was run at least three times.

For the confocal laser scanning microscopy, during the LbL assembly, the last-deposited Ch layer was substituted with fluorescein isothiocyanate-labeled Ch (Ch^{FITC}, 4% of the total amount of Ch in the deposition solution), without any changes in the deposition conditions.

The effect of GO insertion on the promotion of cell adhesive ability of PEMs was studied in composite films with different numbers and localizations of the GO layers in the hydrated polymer matrix. The assembled multilayered films were described as (HA/Ch)_x(GO/Ch)_y(HA/Ch)_z (sub-indexes x, y, and z denote the number of the corresponding bilayers deposited in the listed sequence).

2.2. Cell Culture and Cell Viability Assays

Human umbilical vein endothelial cells (HUVECs) (PromoCell GmbH, Heidelberg, Germany), at passages up to 7, and BALB/3T3 clone A31 (ATCC[®] CCL-163[™]) mouse embryonic (3T3) fibroblasts were routinely grown as a monolayer in T75 tissue culture flasks (Corning Inc., New York, NY, USA). HUVECs were cultured in an endothelial cell growth medium (PromoCell GmbH) with the associated Supplement Mix (PromoCell GmbH), while 3T3 fibroblasts were cultured in Dulbecco's Modified Eagle's Medium (DMEM)—high glucose (4.5 g/L glucose) (Sigma-Aldrich Chemie GmbH, Taufkirchen,

Germany), supplemented with 10% fetal calf serum (Sigma-Aldrich Chemie GmbH, Taufkirchen, Germany) and penicillin/streptomycin (PAA Laboratories) at 37 °C in 5% CO₂. The cells were seeded at a density of 15,000 cells/cm² on the PEM-coated wells of 24-well plates. For positive controls (PCs), an industrially tissue-culture-treated (TCT) polystyrene well plate was used (Corning Inc., New York, NY, USA), and for negative controls (NCs), an untreated polystyrene well plate was used (Greiner Bio-One, Frickenhausen, Germany). HUVECs adhere and proliferate well on the TCT polystyrene and very poorly on the untreated polystyrene.

A resazurin assay was performed to assess cell viability, which allows the quantification of cells with a well-functioning metabolism. HUVECs were seeded onto PEM-coated 24-well plates, as well as plates used as PC and NC. After cultivation for 24 h and 72 h, the medium was replaced with a medium containing 10% (w/w) resazurin (Sigma-Aldrich Chemie GmbH, Taufkirchen, Germany) and incubated for 2 h at 37 °C. In that time, the HUVECs metabolize and reduce Resazurin to Resorufin, resulting in a color change from blue to fluorescent violet. The fluorescence intensity was measured by a fluorescence spectrophotometer (Tecan Austria GmbH, Grödig, Austria) with excitation and emission set at wavelengths of 540 nm and 580 nm, respectively. Cell viability data after 24 h of culture reflect the extent of cell adhesion, and those after 72 h reflect cell proliferation over time.

One set of experiments was performed with coated well plates without any cells to exclude possible resazurin reduction by the surface coatings. Measured absorbance values were subtracted from those assessed in the presence of cells.

2.3. *In Vitro* Cytotoxicity Assay

The cytotoxicity of the PEM coatings was tested in triplicate under sterile conditions according to ISO 10993-5 by the extraction of potentially cytotoxic substances, simulating *in vivo* implantation conditions.

For the extraction tests, PEMs were built on the inner pit surface of a 24-well plate. After drying, 1 mL of the DMEM high glucose cell-culture medium (CCM) with 10% FCS was added to each well. Cytotoxic latex and non-cytotoxic polypropylene (PP) were also tested as positive and negative controls. The well plate was incubated for 72 h in a thermostat at 37 °C and 5% CO₂. In the case that PEM coatings comprise soluble toxic substances, they would dissolve in the CCM, which would become toxic to the cells. After an incubation period of 72 h, the culture medium was instilled into a 96-well plate at 100 µL per well in which 3T3 cells had been pre-seeded. In cytotoxicity experiments, 10,000 cells per well were seeded and incubated with DMEM + 10% FCS + 1% penicillin/streptomycin for 24 h. The vitality of the surviving 3T3 cells was tested using the Neutral Red Uptake (NRU) assay, based on the uptake and concentration of neutral red in the lysosomes of the living cells. When the extracts of studied PEM coatings and reference materials (PC and NC) are evaluated in parallel, the degree of growth inhibition reflects the relative cytotoxicity of the coatings.

2.4. Confocal Laser Scanning Microscopy (CLSM)

Confocal images were obtained using Olympus Fluoview FV1000 confocal laser scanning microscope with the following parameters: objective: UPLSAPO 60× Oil (Numerical aperture: 1.35); confocal aperture: 239 µm; lasers: 405 nm (blue autofluorescence) and 488 nm (FITC) with emission detection ranges between 425 and 475 nm and between 500 and 600 nm, respectively. A total of 50 optical sections of 0.46 µm/slice thickness were captured in the 3D image capturing mode.

2.5. Optical Waveguide Lightmode Spectroscopy (OWLS)

The refractive index and thickness of the deposited layers were measured by means of optical waveguide lightmode spectroscopy (OWLS). The desired multilayer structures were built on the surface of slab optical waveguides equipped with a grating coupler, and the wavelength of the measuring He-Ne laser was 632.8 nm (Melles Griot, 15 mW). The waveguide, composed of a glass substrate, a Si(Ti)O₂ guiding layer, and a coupling grating (Microvacuum Ltd., Budapest, Hungary, $n = 1.8$, $d = 200$ nm), was placed on a rotational stage (Ealing Electro Optics Digital Positioning System), by which the coupling angle could be controlled to an accuracy of 10^{-4} deg [42,43]. The resonance angle, a function of the refractive index of the adlayer, was determined by measuring the outcoupled light at the end of the waveguide by a photomultiplier (Hamamatsu). The light-intensity signal was amplified by a laboratory-built preamplifier and then recorded with a Le Croy 9310L transient digitizer. Considering the relatively small thickness, a four-layer model [44] was used to determine the properties of the multilayer assembly, including the refractive index and the thickness of the adlayer films.

2.6. Ellipsometry

The thickness and refractive index of the PEM films were also evaluated by using a spectroscopic ellipsometer Sentech SE800 (Sentech Instruments GmbH, Berlin, Germany) with a wavelength range from 280 to 850 nm, at an angle of incidence 70 deg. The raw data were fitted by four-layer model accounting for the contributions of the substrate (Si with SiO₂ layer), PEM, and air.

3. Results

3.1. Diffusion of Ch Chains in Control HA/Ch and Composite HA/Ch/GO Multilayers

PEM films comprising a total of 50 bilayers, with the final layer always being Ch^{FITC}, were constructed on glass slides for the purposes of CLSM experiments.

Multilayers with the following composition were built: (HA/Ch)₄₉(HA/Ch^{FITC}) without GO (control); (HA/Ch)₂₅(GO/Ch)(HA/Ch)₂₃(HA/Ch^{FITC}) with a single GO-layer in the middle of the polymer matrix; and (HA/Ch)₃₉(GO/Ch)(HA/Ch)₉(HA/Ch^{FITC}) with a single GO-layer close to the surface of the film. The thickness of the three coatings was in the range of 2.2 to 2.5 μm as estimated from the CLSM images.

The polyelectrolyte multilayers built of HA and Ch are exponentially growing due to the ability of Ch chains to interpenetrate the whole polymer matrix [23]. In our previous works focused on the structure and properties of composite GO-containing films, we assumed that GO layer(s) act as a barrier hindering the interpenetration of Ch chains [38,41]. This assumption was proven here by studying the internal structure of the constructed HA/Ch and HA/Ch/GO films with a single top Ch^{FITC} layer by CLSM and applying 3D optical sectioning. We found that the control (HA/Ch)₅₀ film with FITC-labeled terminal Ch layer showed superior green fluorescence intensity due to Ch^{FITC} interpenetration through the entire polymer matrix (Figure 1A). Blue autofluorescence attributable to the non-FITC-labeled HA/Ch matrix could not be identified. The PE film with a GO layer incorporated in the middle of the polymer matrix (Figure 1B) appeared green in the upper half (i.e., above the GO layer, in contact with the air) and blue in the bottom half (below the GO layer, in contact with the glass substrate). The FITC-labeled green matrix and the non-labeled blue matrix were equally thick (about 1.1–1.2 μm each). This indicates that even a single GO layer is able to completely hinder the interpenetration of Ch chains. The film with GO layer located close to the outer PEM/air interface had the weakest green fluorescence and the thinnest fluorescent layer on the upper surface. The bulk of the polymer matrix appeared blue fluorescent since there are no Ch^{FITC} chains passed below the GO barrier (Figure 1C).

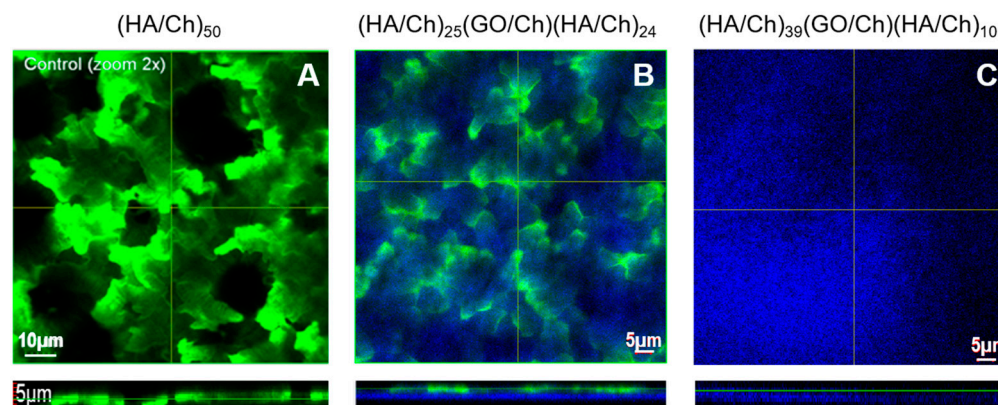


Figure 1. CLSM images—both top and cross-sectional views—of (HA/Ch)₅₀ film (A) and composite HA/Ch/GO films with one GO layer in the middle of the film (B) or close to the film surface (C), all with FITC-labeled terminal Ch layer.

The top-view images in Figure 1 show a trend of a significant decrease in surface roughness as the GO layer approaches the surface of the coating. The high surface roughness of the (HA/Ch)₅₀ film (Figure 1A) is consistent with our earlier finding that the roughness of HA/Ch multilayers increases exponentially with the number of bilayers, respectively with the thickness [45]. The GO layer incorporated in the middle of the composite HA/Ch film hinders the exponential growth and interpenetration of Ch chains and acts as a new substrate on which a new HA/Ch film grows. The roughness of this coating does not correspond to a 50-bilayer HA/Ch film but rather to a 25-bilayer film and is, therefore, much lower. Similarly, the surface roughness of the (HA/Ch)₃₉(GO/Ch)(HA/Ch)₁₀ coating corresponds to 10-bilayer HA/Ch film and is very low.

3.2. Thickness and Refractive Index of Composite HA/Ch/GO Films

In this study, OWLS and ellipsometry were used to estimate the thickness and refractive index of HA/Ch and composite HA/Ch/GO films. The OWLS thickness of the control (HA/Ch)₁₀ film is equivalent to that of the composite film with seven GO layers (Table 1). Although the ellipsometric thickness appears slightly higher than that of OWLS, it is also independent of the composition of the PEM. The refractive index of the (HA/Ch)₁₀ film assessed by OWLS was 1.58, in agreement with a value previously reported for (HA/Ch)₅ film [23]. The complex refractive index of GO flakes estimated by spectroscopic ellipsometry is 1.96 [46]. The OWLS refractive index of the composite HA/Ch/GO film with seven GO layers is 1.71 (Table 1); therefore, it increases with the incorporation of GO layers. Although the ellipsometric refractive index is somewhat higher than the OWLS one, it follows the same trend, i.e., it increases with the number of GO layers owing to the integration in the PEMs of a material with a much higher inherent refractive index.

Table 1. Comparison of the thickness and refractive index of HA/Ch and composite HA/Ch/GO films acquired by OWLS and spectroscopic ellipsometry.

Sample	OWLS		Ellipsometry	
	Thickness (nm)	Refractive Index	Thickness (nm)	Refractive Index
(HA/Ch) ₁₀	75.3 ± 0.3	1.58 ± 0.01	92.0 ± 2.3	1.63 ± 0.02
(HA/Ch) ₉ GO			84.4 ± 3.0	1.70 ± 0.03
(HA/Ch) ₉ (GO/Ch)			90.2 ± 2.5	1.72 ± 0.04
(HA/Ch) ₂ (GO/Ch) ₇ (HA/Ch)	74.0 ± 1.0	1.71 ± 0.01	90.0 ± 2.5	1.80 ± 0.02

3.3. Cell Adhesion and Growth on Composite HA/Ch/GO Films

In our recent works, we showed that the incorporation of GO in different amounts and positions in biodegradable HA/Ch multilayers does not affect thickness and hydrophilicity but causes a significant change in surface morphology and roughness [38,41]. The altered surface properties, in turn, affect the protein adsorption and adhesion of human blood platelets on the composite GO/HA/Ch films [38]. In this study, we go further, exploring the possibility of controlling the adhesion and proliferation of fibroblasts and endothelial cells on material surfaces by composite coatings with different number and localization of the GO layers.

The control (HA/Ch)₁₀ film without GO completely prevents the adhesion and proliferation of HUVECs (Figure 2), one of the best characterized and most frequently used endothelial cells in the study of tissue–biomaterial interactions, especially when biomaterials are in contact with blood vessels [47]. In contrast, all composite PEMs support the adhesion of HUVECs to a different extent depending on the number and localization of GO layers in the PEM matrix. On all HA/Ch/GO coatings, adherent cells were viable and proliferated over time. The (HA/CH)₉GO film with surface-exposed GO-layer promotes HUVEC's adhesion to the greatest extent, almost equaling that of the positive control. The addition of just one top Ch layer in the (HA/Ch)₉(GO/Ch) film reduced the number of adherend cells by about 15% compared to the (HA/CH)₉GO film. The composite coating with seven incorporated GO layers suppressed cell adhesion with 70% and cell proliferation with 50% compared to the positive control.

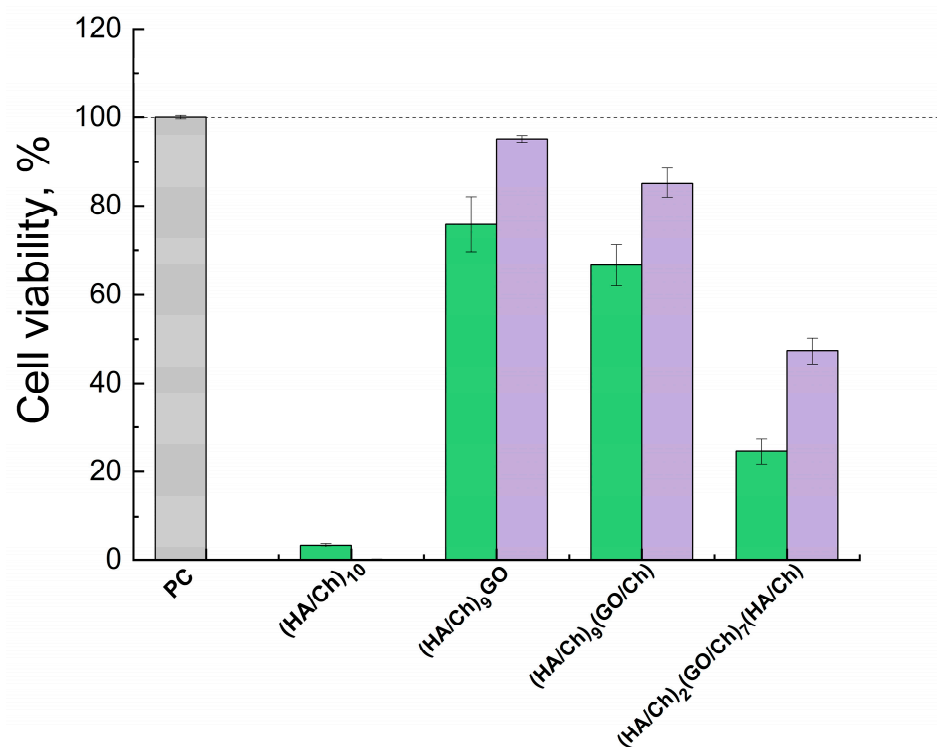


Figure 2. HUVEC viability on the control (HA/Ch)₁₀ film and different composite films containing GO layer(s), relative to that on TCT well plate (PC). Cells were cultured for 24 h (green) and 72 h (violet). Data for 24 h of cell culture reflect the number of adherend cells and these for 72 h reflect the extent of cell proliferation.

The cell behavior of 3T3 fibroblasts on the same coatings appeared similar to that of HUVECs (Figure 3). Cell adhesion on the control (HA/Ch)₁₀ film was reduced by 75% relative to the positive control. All composite coatings demonstrated significantly better cell adhesive ability than the control film without GO. The (HA/Ch)₉GO and (HA/Ch)₉(GO/Ch) films demonstrated improved cell adhesion and proliferation as compared to the positive

control, while the coating with seven incorporated GO layers reduced cell proliferation by ca. 12%.

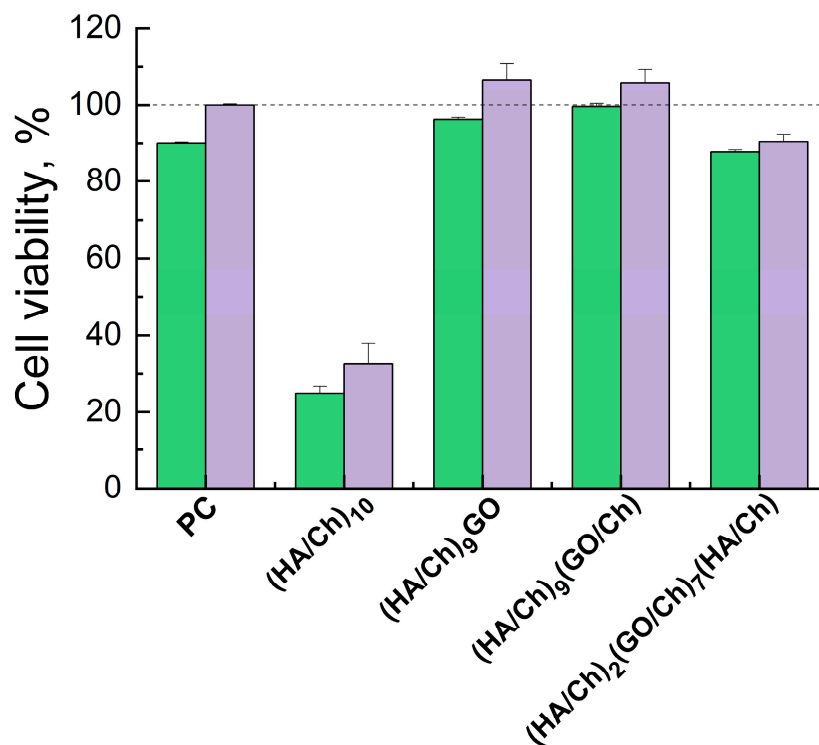


Figure 3. 3T3 fibroblasts viability on control (HA/Ch)₁₀ and different composite films containing GO-layers, relative to that on TCT well plates (PC). Cells were cultured for 24 h (green) and 72 h (violet). Data for 24 h of cell culture reflect the number of adherent cells, and those for 72 h reflect the extent of cell proliferation.

3.4. Cytotoxicity of Composite HA/Ch/GO Films

The biocompatibility of medical devices and their constituent components and materials is of great importance to ensure their safety. Here, the cytotoxicity of the PEM coatings, with and without GO incorporated, was examined according to the standard ISO 10993-5, with a growth inhibition test with 3T3 mouse fibroblasts. The ISO 10993-5 cytotoxicity assay assesses the release of extractable cytotoxic substances from the coatings, and the results are consistent with those of the animal toxicity tests.

The NRU test applied here for the quantitative estimation of living cells relies on the linear relationship between the number of the viable cells and the absorbance signal. Figure 4 shows the cell viability of a 3T3 cell line exposed to an undiluted extract from the control (HA/Ch)₁₀ and the composite HA/Ch/GO coatings with different composition, as well as from the negative control (NC, non-cytotoxic polypropylene) and positive control (PC, toxic latex). As expected, the NC shows 100% cell viability (0% growth inhibition), while the PC shows 0% cell viability, hence 100% toxicity. According to ISO 10993-5, if the exposure of cells to a fully concentrated sample extract reduces cell viability by less than 30%, then the material is considered non-cytotoxic. The results in Figure 4 indicated that HA/Ch/GO coatings do not exert growth inhibitory and cytotoxic effects on 3T3 mouse fibroblasts. The viability rate of fibroblasts was reduced by up to 3% when exposed to 100% extract from either coating. Therefore, the addition of GO to the biocompatible HA/Ch coatings did not affect their non-cytotoxicity.

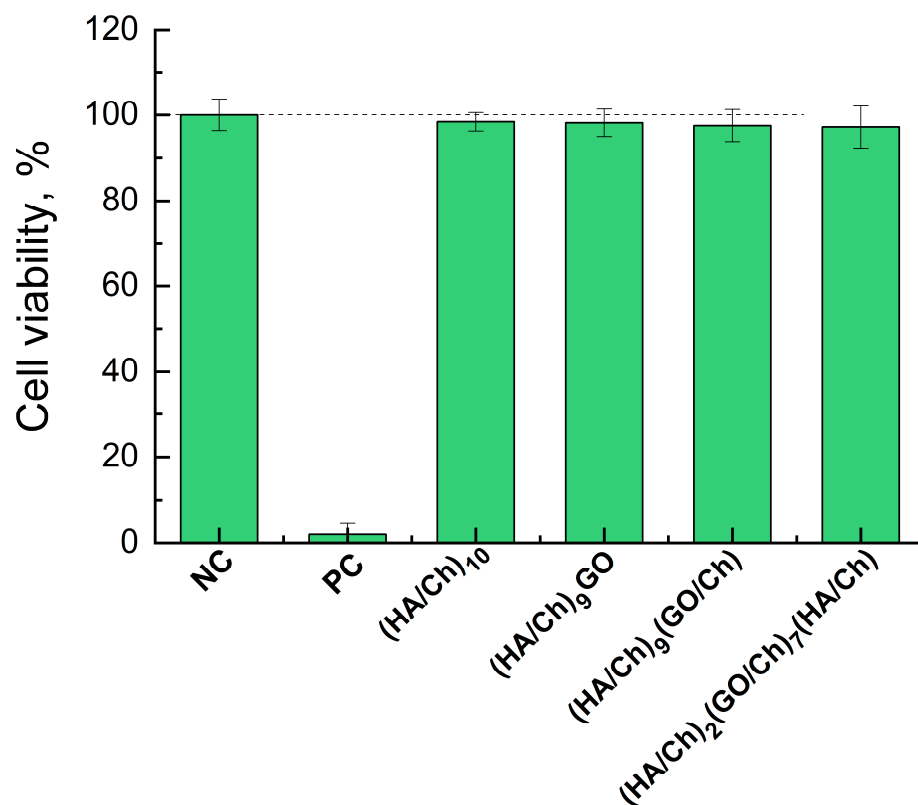


Figure 4. Cell viability of 3T3 fibroblasts assessed by NRU assay after 24 h exposure to 100% extraction medium from the PEM coatings. Polypropylene is used as a negative control (NC) and latex as a positive control (PC).

4. Discussion

Controlling cell adhesion, proliferation, and function on material surfaces is a challenge in implantology, tissue engineering, and regenerative medicine as it is highly dependent on many factors, such as surface chemistry, charge, morphology, hydrophilicity, and stiffness [48]. In the present work, we assessed the effect of the incorporation of one or more GO layers in HA/Ch multilayers on the adhesion of HUVECs and 3T3 cells. HA/Ch multilayers are well known for their biocompatibility and non-cytotoxicity, however combined with poor mechanical and cell adhesive properties [23].

Owing to its unique characteristics (physical, mechanical, and electrical), GO is a promising candidate for biomedical applications; therefore, its cytotoxicity on mammalian cells is currently undergoing intensive research, yielding contradictory data thus far. While there is already a consensus on the cytotoxicity of GO sheets in suspension, this is not the case for immobilized GO sheets. The effect of GO flakes in suspension on the viability of human erythrocytes, skin fibroblast cells, and lung cancer cell line A549 was found to depend on both the concentration and the lateral dimensions of GO sheets [49,50]. The incubation of suspended human red blood cells and adherent human skin fibroblasts with GO suspension resulted in the formation of a GO shield which severely restricted the cell's access to the nutrient, and the integrity of this shield was strongly dependent on the GO suspension concentration and the size of GO flakes [49]. In another in vitro and in vivo study, GO suspension proved to have no toxicity against human fibroblast cells at a concentration less than 20 $\mu\text{g}/\text{mL}$ but was definitely toxic at concentrations above 50 $\mu\text{g}/\text{mL}$ [51]. The in vivo study demonstrated that a single injection with 0.1 mg and 0.25 mg suspended GO sheets did not induce obvious harm to mice; however, the application of 0.4 mg provoked chronic toxicity and mice death [51]. On the contrary, Chang et al. [52] found that GO does not enter A549 cells and hardly changes the morphology, viability, mortality, and membrane integrity of cells, despite inducing a dose- and size-

dependent oxidative stress and slight loss of cell viability at concentrations higher than 50 $\mu\text{g}/\text{mL}$ and small sheets size ($160 \pm 90 \text{ nm}$).

We have found that when immobilized into or on the surface of the HA/Ch multilayer, GO does not exert any cell inhibitory effects even at high concentrations (Figure 4). This finding is consistent with a study reporting that GO sheets immobilized on a glass coverslip showed high biocompatibility and did not affect the behavior, namely the adhesion, proliferation, spreading, and focal adhesion of NIH-3T3 fibroblasts, and even improved the gene transfection efficiency [53]. Our results are also consistent with data stating that coating GO sheets with chitosan eliminated their hemolytic activity [49].

The results also demonstrated that both HUVECs and 3T3 cells adhere and proliferate profoundly better on the HA/Ch/GO nanocomposite films compared to the HA/Ch films without GO (Figures 3 and 4). A recent study revealed that the surface modification of porous polymer-carbon fibers with GO changed the micro-roughness and nanostructure which, in turn, improved the attachment and proliferation of bone marrow mesenchymal stem cells and the new bone formation both *in vitro* and *in vivo* [54]. In our previous systematic investigation of the physicochemical properties of HA/Ch/GO coatings, we showed that the average roughness, thickness, and hydrophilicity of the control (HA/CH)₁₀ film and composite GO-containing films were quite similar [39], yet, here, they demonstrated remarkable differences in terms of cell adhesion.

Polysaccharide-based multilayers are well known for their resistance to the adhesion of serum proteins, thrombo-resistance, antifouling, and anti-cell adhesive properties [55,56], all due to the high hydration and low elastic modulus of these multilayers. The poor adhesion of HUVECs (Figure 3) and 3T3 cells (Figure 4) on the (HA/Ch)₁₀ multilayer that we observe here is consistent with these findings. Furthermore, we showed that the cellular response to (HA/Ch)₁₀ could be improved by increasing the film density by embedding one or more extremely thin but rather stiff GO layer(s). As expected, the refractive index of the coatings studied here, which reflects their density, increases with increasing the number of incorporated GO layers (Table 1). However, cell adhesion does not increase in the same order. In fact, the results imply that incorporating the GO layer close to the surface enhances the cell adhesive ability. This is the factor shaping the pro-adhesive properties of the PEMs in the following order: (HA/Ch)₁₀ < (HA/Ch)₂(GO/Ch)₇(HA/Ch) < (HA/Ch)₉(GO/Ch) \leq (HA/Ch)₉GO \approx PC. GO layers demonstrate extremely high stiffness (Young's modulus ca. 200 GPa [57]), in contrast to highly hydrated HA/Ch multilayers (Young's modulus ca. 150 kPa [45]). Therefore, the overall stiffness of HA/Ch/GO composite films should increase with the number of embedded GO layers as already shown for PSS/PAH/GO films [58]. However, cell adhesion did not improve with increasing the number of GO layers, correspondingly increasing the stiffness of the films. The cellular response to the coatings is enhanced as the GO layer approaches their surface (data in Figures 3 and 4). The surface of a material refers to its outermost layer, which can have distinct properties influencing its interaction with other materials. In this sense, the surface stiffness of the coatings might differ from their overall stiffness and, more specifically, in our case, is defined by the composition of the last few layers. The surface stiffness should increase with GO inclusion closer to the surface. Therefore, the enhancement of HUVEC and 3T3 cell adhesion and growth is triggered by the increase in surface rigidity which was the most favorable for the PEM with a surface-exposed GO layer.

Capping the HA/Ch multilayer with a continuous GO layer with a very high elastic modulus (coating (HA/Ch)₉GO in Figures 3 and 4) resulted in a substantial improvement in the cell adhesion and proliferation, reaching those on the TCT plate, considered the gold standard. The addition of just one top Ch layer (coating (HA/Ch)₉(GO/Ch)) reduced the number of adherent HUVECs by about 15% compared to the (HA/CH)₉GO film, while the composite coating with seven incorporated GO layers reduced the HUVEC's adhesion with 70% and the cell proliferation with 50% compared to the positive control. Such behavior suggests that the cells sense only the last few nm close to the surface but not the whole volume of the coating. Although the coating with seven GO layers is the stiffest among

the three composite coatings, the top 5–10 nm of the film is built of polysaccharide layers, which are poorly cell adhesive.

Surface charge has no determining effect on cell adhesion, judging by the three coatings with the same top Ch layer, which show significantly different cell viability, while, at the same time, the (HA/Ch)₉GO and (HA/Ch)₉(GO/Ch) coatings having a different final layer charge, show similar cell viability.

Our results imply that during adhesion, cells primarily sense the surface properties of a material but not the bulk ones. The process of cell adhesion involves specific interactions between molecules on the cell membrane and ligands present on the surface of the material [59]. These interactions play a crucial role in the initial attachment of cells to a material [60]. While the surface properties are vital, the bulk composition can indirectly influence the adhesion through factors like material overall stiffness and elasticity, hydration, etc. [61]. However, the primary sensing mechanism occurs at the material's surface. This behavior follows the same trend for endothelial cells (HUVECs) and fibroblasts (3T3 cells), but it is more pronounced for HUVECs, which are more sensitive towards apoptosis stimuli [62].

5. Conclusions

A simple yet general approach to improve the biocompatibility of biomaterials by controlling cellular response to their surfaces is presented. It consists of surface modification by depositing an extremely thin (ca. 75 nm measured by OWLS and ca. 90 nm measured by ellipsometry) composite coating. The coating is based on a polyelectrolyte multilayer, made of the two most attractive natural polysaccharides, hyaluronic acid, and chitosan, which stands out for its non-toxicity, biodegradability, and biofilm repulsion but, at the same time completely resistance to cell adhesion.

Both terminating the HA/Ch multilayer with a single GO monolayer or embedding a different number of GO layers into the HA/Ch matrix modify the adhesion and proliferation of fibroblasts and endothelial cells over the entire range of zero (for the control HA/Ch coating without GO) up to 100%, equal to the gold standard for cellular response (for the composite HA/Ch/GO coating with GO top layer). Regardless of the number and localization of GO layer(s), their incorporation had a positive effect in terms of cell adhesion, proliferation, and viability, compared to HA/Ch multilayer films without GO, without compromising the cytotoxicity at all.

Author Contributions: Conceptualization, T.A. and S.G.T.; methodology, A.D. and M.B.; formal analysis, L.F.; investigation, A.R., I.I., L.F. and F.A.; resources, R.K. and A.D.; data curation, O.J.; writing—original draft preparation, T.A.; writing—review and editing, S.G.T. and R.K.; visualization, O.J.; supervision, T.A., S.G.T. and M.B.; project administration, R.K.; funding acquisition, R.K. All authors have read and agreed to the published version of the manuscript.

Funding: The authors gratefully acknowledge the funding by the German Research Foundation (Deutsche Forschungsgemeinschaft, DFG) for the subproject 2 within the Research Unit 5250 “Permanent and bioresorbable implants with tailored functionality” (No. 449916462). F.A. is supported by Horizon 2020 Framework Programme 739593.

Institutional Review Board Statement: Not applicable.

Informed Consent Statement: Not applicable.

Data Availability Statement: Data is provided upon request.

Conflicts of Interest: The authors declare no conflict of interest.

References

1. Petrilă, L.M.; Bucatariu, F.; Mihai, M.; Teodosiu, C. Polyelectrolyte Multilayers: An Overview on Fabrication, Properties, and Biomedical and Environmental Applications. *Materials* **2021**, *14*, 4152. [[CrossRef](#)] [[PubMed](#)]
2. Singh, A.V.; Ferri, M.; Tamplenizza, M.; Borghi, F.; Divitini, G.; Ducati, C.; Lenardi, C.; Piazzoni, C.; Merlini, M.; Podestà, A.; et al. Bottom-up engineering of the surface roughness of nanostructured cubic zirconia to control cell adhesion. *Nanotechnology* **2012**, *23*, 475101. [[CrossRef](#)] [[PubMed](#)]
3. Ranella, A.; Barberoglou, M.; Bakogianni, S.; Fotakis, C.; Stratakis, E. Tuning cell adhesion by controlling the roughness and wettability of 3d micro/nano silicon structures. *Acta Biomater.* **2010**, *6*, 2711–2720. [[CrossRef](#)]
4. Ventre, M.; Natale, C.F.; Rianna, C.; Netti, P.A. Topographic cell instructive patterns to control cell adhesion, polarization and migration. *J. R. Soc. Interface* **2014**, *11*, 20140687. [[CrossRef](#)]
5. Zhou, J.; Zhang, X.; Sun, J.; Dang, Z.; Li, J.; Li, X.; Chen, T. The effects of surface topography of nanostructure arrays on cell adhesion. *Phys. Chem. Chem. Phys.* **2018**, *20*, 22946. [[CrossRef](#)]
6. Discher, D.E.; Janmey, P.; Wang, Y.-L. Tissue Cells Feel and Respond to the Stiffness of Their Substrate. *Science* **2005**, *310*, 1139. [[CrossRef](#)]
7. Yeung, T.; Georges, P.C.; Flanagan, L.A.; Marg, B.; Ortiz, M.; Funaki, M.; Zahir, N.; Ming, W.; Weaver, V.; Janmey, P.A. Effects of substrate stiffness on cell morphology, cytoskeletal structure, and adhesion. *Cell Motil. Cytoskelet.* **2005**, *60*, 24. [[CrossRef](#)]
8. Sun, M.; Chi, G.; Li, P.; Lv, S.; Xu, J.; Xu, Z.; Xia, Y.; Tan, Y.; Xu, J.; Li, L.; et al. Effects of Matrix Stiffness on the Morphology, Adhesion, Proliferation and Osteogenic Differentiation of Mesenchymal Stem Cells. *Int. J. Med. Sci.* **2018**, *15*, 257. [[CrossRef](#)]
9. Metwally, S.; Stachewicz, U. Surface potential and charges impact on cell responses on biomaterials interfaces for medical applications. *Mater. Sci. Eng. C* **2019**, *104*, 109883. [[CrossRef](#)]
10. Guo, S.; Zhu, X.; Li, M.; Shi, L.; Ong, J.L.T.; Jańczewski, D.; Neoh, K.G. Parallel Control over Surface Charge and Wettability Using Polyelectrolyte Architecture: Effect on Protein Adsorption and Cell Adhesion. *ACS Appl. Mater. Interfaces* **2016**, *8*, 30552–30563. [[CrossRef](#)]
11. Kennedy, S.B.; Washburn, N.R.; Simon, C.G.; Amis, E.J. Combinatorial screen of the effect of surface energy on fibronectin-mediated osteoblast adhesion, spreading and proliferation. *Biomaterials* **2006**, *27*, 3817–3824. [[CrossRef](#)] [[PubMed](#)]
12. Köstler, S.; Delgado, A.V.; Ribitsch, V. Surface thermodynamic properties of polyelectrolyte multilayers. *J. Colloid Interface Sci.* **2005**, *286*, 339. [[CrossRef](#)]
13. Gong, X. Controlling surface properties of polyelectrolyte multilayers by assembly pH. *Phys. Chem. Chem. Phys.* **2013**, *15*, 10459. [[CrossRef](#)] [[PubMed](#)]
14. Towle, E.G.; Ding, I.; Peterson, A.M. Impact of molecular weight on polyelectrolyte multilayer assembly and surface properties. *J. Colloid Interface Sci.* **2020**, *570*, 135. [[CrossRef](#)] [[PubMed](#)]
15. Lotfi, M.; Nejib, M.; Naceur, M. Cell Adhesion to Biomaterials: Concept of Biocompatibility. In *Advances in Biomaterials Science and Biomedical Applications*; Pignatello, R., Ed.; IntechOpen: Rijeka, Croatia, 2013. [[CrossRef](#)]
16. Dennaoui, H.; Chouery, E.; Rammal, H.; Abdel-Razzak, Z.; Harmouch, C. Chitosan/hyaluronic acid multilayer films are biocompatible substrate for Wharton's jelly derived stem cells. *Stem Cell Investig.* **2018**, *5*, 47. [[CrossRef](#)] [[PubMed](#)]
17. Vigani, B.; Rossi, S.; Sandri, G.; Bonferoni, M.C.; Caramella, C.M.; Ferrari, F. Hyaluronic acid and chitosan-based nanosystems: A new dressing generation for wound care. *Expert Opin. Drug Deliv.* **2019**, *16*, 715. [[CrossRef](#)] [[PubMed](#)]
18. Hartmann, H.; Hossfeld, S.; Schlosshauer, B.; Mittnacht, U.; Pêgo, A.P.; Dauner, M.; Doser, M.; Stoll, D.; Krastev, R. Hyaluronic acid/chitosan multilayer coatings on neuronal implants for localized delivery of siRNA nanoplexes. *J. Control. Release* **2013**, *168*, 289. [[CrossRef](#)]
19. Park, H.; Choi, B.; Hu, J.; Lee, M. Injectable chitosan hyaluronic acid hydrogels for cartilage tissue engineering. *Acta Biomater.* **2013**, *9*, 4779–4786. [[CrossRef](#)] [[PubMed](#)]
20. Deng, Y.; Ren, J.; Chen, G.; Li, G.; Wu, X.; Wang, G.; Gu, G.; Li, J. Injectable in situ cross-linking chitosan-hyaluronic acid based hydrogels for abdominal tissue regeneration. *Sci. Rep.* **2017**, *7*, 2699. [[CrossRef](#)]
21. Correia, C.R.; Moreira-Teixeira, L.S.; Moroni, L.; Reis, R.L.; van Blitterswijk, C.A.; Karperien, M.; Mano, J.F. Chitosan scaffolds containing hyaluronic acid for cartilage tissue engineering. *Tissue Eng. Part C Methods* **2011**, *17*, 717. [[CrossRef](#)]
22. Schneider, A.; Richert, L.; Francius, G.; Voegel, J.-C.; Picart, C. Elasticity, biodegradability and cell adhesive properties of chitosan/hyaluronan multilayer films. *Biomed. Mater.* **2007**, *2*, S45. [[CrossRef](#)]
23. Richert, L.; Lavallo, P.; Payan, E.; Shu, X.Z.; Prestwich, G.D.; Stoltz, J.-F.; Schaaf, P.; Voegel, J.-C.; Picart, C. Layer by layer buildup of polysaccharide films: Physical chemistry and cellular adhesion aspects. *Langmuir* **2004**, *20*, 448. [[CrossRef](#)]
24. Jou, C.-H.; Yuan, L.; Lin, S.-M.; Hwang, M.-C.; Chou, W.-L.; Yu, D.-G.; Yang, M.-C. Biocompatibility and antibacterial activity of chitosan and hyaluronic acid immobilized polyester fibers. *J. Appl. Polym. Sci.* **2007**, *104*, 220. [[CrossRef](#)]
25. Hoyo-Gallego, S.D.; Pérez-Álvarez, L.; Gómez-Galván, F.; Lizundia, E.; Kuritka, I.; Sedlarik, V.; Laza, J.M.; Vila-Vilela, J.L. Construction of antibacterial poly(ethylene terephthalate) films via layer by layer assembly of chitosan and hyaluronic acid. *Carbohydr. Polym.* **2016**, *143*, 35. [[CrossRef](#)] [[PubMed](#)]
26. Croll, T.I.; O'Connor, A.J.; Stevens, G.W.; Cooper-White, J.J. A Blank Slate? Layer-by-Layer Deposition of Hyaluronic Acid and Chitosan onto Various Surfaces. *Biomacromolecules* **2006**, *7*, 1610–1622. [[CrossRef](#)] [[PubMed](#)]
27. Yu, W.; Koc, J.; Finlay, J.A.; Clarke, J.L.; Clare, A.S.; Rosenhahn, A. Layer-by-layer constructed hyaluronic acid/chitosan multilayers as antifouling and fouling-release coatings. *Biointerphases* **2019**, *14*, 051002. [[CrossRef](#)]

28. Almalik, A.; Benabdelkamel, H.; Masood, A.; Alanazi, I.O.; Alradwan, I.; Majrashi, M.A.; Alfadda, A.A.; Alghamdi, W.M.; Alrabiah, H.; Tirelli, N.; et al. Hyaluronic Acid Coated Chitosan Nanoparticles Reduced the Immunogenicity of the Formed Protein Corona. *Sci. Rep.* **2017**, *7*, 10542. [[CrossRef](#)]
29. Etienne, O.; Schneider, A.; Taddei, C.; Richert, L.; Schaaf, P.; Voegel, J.-C.; Egles, C.; Picart, C. Degradability of Polysaccharides Multilayer Films in the Oral Environment: An In Vitro and In Vivo Study. *Biomacromolecules* **2005**, *6*, 726–733. [[CrossRef](#)]
30. Schneider, A.; Francius, G.; Obeid, R.; Schwinté, P.; Hemmerlé, J.; Frisch, B.; Schaaf, P.; Voegel, J.-C.; Senger, B.; Picart, C. Polyelectrolyte Multilayers with a Tunable Young's Modulus: Influence of Film Stiffness on Cell Adhesion. *Langmuir* **2006**, *22*, 1193. [[CrossRef](#)]
31. Moshnikova, A.B.; Afanasyev, V.N.; Proussakova, O.V.; Chernyshov, S.; Gogvadze, V.; Beletsky, I.P. Cytotoxic activity of 1-ethyl-3-(3-dimethylaminopropyl)-carbodiimide is underlain by DNA interchain cross-linking. *Cell. Mol. Life Sci.* **2006**, *63*, 229. [[CrossRef](#)]
32. Schmidt, S.; Madaboosi, N.; Uhlig, K.; Köhler, D.; Skirtach, A.; Duschl, C.; Möhwald, H.; Volodkin, D.V. Control of Cell Adhesion by Mechanical Reinforcement of Soft Polyelectrolyte Films with Nanoparticles. *Langmuir* **2012**, *28*, 7249. [[CrossRef](#)]
33. Almeida, A.C.; Vale, A.C.; Reis, R.L.; Alves, N.M. Bioactive and adhesive properties of multilayered coatings based on catechol-functionalized chitosan/hyaluronic acid and bioactive glass nanoparticles. *Int. J. Biol. Macromol.* **2020**, *157*, 119–134. [[CrossRef](#)]
34. Sun, Y.; Zhang, K.; Deng, R.; Ren, X.; Wu, C.; Li, J. Tunable stiffness of graphene oxide/polyacrylamide composite scaffolds regulates cytoskeleton assembly. *Chem. Sci.* **2018**, *9*, 6516. [[CrossRef](#)]
35. Abalymov, A.A.; Parakhonskiy, B.V.; Skirtach, A.G. Colloids-at-surfaces: Physicochemical approaches for facilitating cell adhesion on hybrid hydrogels. *Colloids Surf. A Physicochem. Eng. Asp.* **2020**, *603*, 125185. [[CrossRef](#)]
36. Liao, C.; Li, Y.; Tjong, S.C. Graphene Nanomaterials: Synthesis, Biocompatibility, and Cytotoxicity. *Int. J. Mol. Sci.* **2018**, *19*, 3564. [[CrossRef](#)] [[PubMed](#)]
37. Park, S.; Mohanty, N.; Suk, J.W.; Nagaraja, A.; An, J.; Piner, R.D.; Cai, W.; Dreyer, D.R.; Berry, V.; Ruoff, R.S. Biocompatible, Robust Free-Standing Paper Composed of a TWEEN/Graphene Composite. *Adv. Mater.* **2010**, *22*, 1736–1740. [[CrossRef](#)]
38. Andreeva, T.D.; Stoichev, S.; Taneva, S.G.; Krastev, R. Hybrid graphene oxide/polysaccharide nanocomposites with controllable surface properties and biocompatibility. *Carbohydr. Polym.* **2018**, *181*, 78. [[CrossRef](#)]
39. Wilson, C.J.; Clegg, R.E.; Leavesley, D.I.; Pearcy, M.J. Mediation of Biomaterial–Cell Interactions by Adsorbed Proteins: A Review. *Tissue Eng.* **2005**, *11*, 1–18. [[CrossRef](#)]
40. Zhang, M.; Yin, B.-C.; Wang, X.-F.; Ye, B.-C. Interaction of peptides with graphene oxide and its application for real-time monitoring of protease activity. *Chem. Commun.* **2011**, *47*, 2399–2401. [[CrossRef](#)] [[PubMed](#)]
41. Andreeva, T.D.; Dér, A.; Kelemen, L.; Krastev, R.; Taneva, S.G. Modulation of the internal structure and surface properties of natural and synthetic polymer matrices by graphene oxide doping. *Polym. Adv. Technol.* **2020**, *31*, 1562. [[CrossRef](#)]
42. Ormos, P.; Fábíán, L.; Oroszi, L.; Wolff, E.K.; Ramsden, J.J.; Dér, A. Protein-based integrated optical switching and modulation. *Appl. Phys. Lett.* **2002**, *80*, 4060. [[CrossRef](#)]
43. Fábíán, L.; Wolff, E.K.; Oroszi, L.; Ormos, P.; Dér, A. Fast integrated optical switching by the protein bacteriorhodopsin. *Appl. Phys. Lett.* **2010**, *97*, 142. [[CrossRef](#)]
44. Tiefenthaler, K.; Lukosz, W. Sensitivity of grating couplers as integrated-optical chemical sensors. *J. Opt. Soc. Am. B* **1989**, *6*, 209. [[CrossRef](#)]
45. Andreeva, T.D.; Hartmann, H.; Taneva, S.G.; Krastev, R. Regulation of the growth, morphology, mechanical properties and biocompatibility of natural polysaccharide-based multilayers by Hofmeister anions. *J. Mater. Chem. B* **2016**, *4*, 7092. [[CrossRef](#)]
46. Schmiedova, V.; Pospisil, J.; Kovalenko, A.; Ashcheulov, P.; Fekete, L.; Cubon, T.; Kotrusz, P.; Zmeskal, O.; Weiter, M. Physical Properties Investigation of Reduced Graphene Oxide Thin Films Prepared by Material Inkjet Printing. *J. Nanomater.* **2017**, *2017*, 3501903. [[CrossRef](#)]
47. Hauser, S.; Jung, F.; Pietzsch, J. Human Endothelial Cell Models in Biomaterial Research. *Trends Biotechnol.* **2017**, *35*, 265–277. [[CrossRef](#)] [[PubMed](#)]
48. Gribova, V.; Auzely-Velty, R.; Picart, C. Polyelectrolyte multilayer assemblies on materials surfaces: From cell adhesion to tissue engineering. *Chem. Mater.* **2012**, *24*, 854. [[CrossRef](#)] [[PubMed](#)]
49. Liao, K.-H.; Lin, Y.-S.; Macosko, C.W.; Haynes, C.L. Cytotoxicity of Graphene Oxide and Graphene in Human Erythrocytes and Skin Fibroblasts. *ACS Appl. Mater. Interfaces* **2011**, *3*, 2607. [[CrossRef](#)]
50. Hu, W.; Peng, C.; Luo, W.; Lv, M.; Li, X.; Li, D.; Huang, Q.; Fan, C. Graphene-Based Antibacterial Paper. *ACS Nano* **2010**, *4*, 4317. [[CrossRef](#)]
51. Wang, K.; Ruan, J.; Song, H.; Zhang, J.; Wo, Y.; Cui, D. Biocompatibility of Graphene Oxide. *Nanoscale Res. Lett.* **2011**, *6*, 8. [[CrossRef](#)]
52. Chang, Y.; Yang, S.-T.; Liu, J.-H.; Dong, E.; Wang, Y.; Cao, A.; Wang, H. In vitro toxicity evaluation of graphene oxide on A549 cells. *Toxicol. Lett.* **2011**, *200*, 201. [[CrossRef](#)] [[PubMed](#)]
53. Ryoo, S.-R.; Kim, Y.-K.; Kim, M.-H.; Min, D.-H. Behaviors of NIH-3T3 Fibroblasts on Graphene/Carbon Nanotubes: Proliferation, Focal Adhesion, and Gene Transfection Studies. *ACS Nano* **2010**, *4*, 6587. [[CrossRef](#)] [[PubMed](#)]
54. Qin, W.; Li, Y.; Ma, J.; Liang, Q.; Cui, X.; Jia, H.; Tang, B. Osseointegration and biosafety of graphene oxide wrapped porous CF/PEEK composites as implantable materials: The role of surface structure and chemistry. *Dent. Mater.* **2020**, *36*, 1289. [[CrossRef](#)] [[PubMed](#)]

55. Crouzier, T.; Boudou, T.; Picart, C. Polysaccharide-based polyelectrolyte multilayers. *Curr. Opin. Coll. Int. Sci.* **2010**, *15*, 417. [[CrossRef](#)]
56. Thierry, B.; Winnik, F.M.; Merhi, Y.; Silver, J.; Tabrizian, M. Bioactive Coatings of Endovascular Stents Based on Polyelectrolyte Multilayers. *Biomacromolecules* **2003**, *4*, 1564–1571. [[CrossRef](#)]
57. Suk, J.W.; Piner, R.D.; An, J.; Ruoff, R.S. Mechanical properties of monolayer graphene oxide. *ACS Nano* **2010**, *4*, 6557. [[CrossRef](#)]
58. Qi, W.; Xue, Z.; Yuan, W.; Wang, H. Layer-by-layer assembled graphene oxide composite films for enhanced mechanical properties and fibroblast cell affinity. *J. Mater. Chem. B* **2014**, *2*, 325. [[CrossRef](#)] [[PubMed](#)]
59. Neděla, O.; Slepíčka, P.; Švorčík, V. Surface Modification of Polymer Substrates for Biomedical Applications. *Materials* **2017**, *10*, 1115. [[CrossRef](#)] [[PubMed](#)]
60. Howlett, C.R.; Evans, M.D.M.; Walsh, W.R.; Johnson, G.; Steele, J.G. Mechanism of initial attachment of cells derived from human bone to commonly used prosthetic materials during cell culture. *Biomaterials* **1994**, *15*, 213–222. [[CrossRef](#)]
61. Cai, S.; Wu, C.; Yang, W.; Liang, W.; Yu, H.; Liu, L. Recent advance in surface modification for regulating cell adhesion and behaviors. *Nanotechnol. Rev.* **2020**, *9*, 971. [[CrossRef](#)]
62. Hoffmann, J.; Haendeler, J.; Aicher, A.; Rössig, L.; Vasa, M.; Zeiher, A.M.; Dimmeler, S. Aging enhances the sensitivity of endothelial cells toward apoptotic stimuli: Important role of nitric oxide. *Circ. Res.* **2001**, *89*, 709. [[CrossRef](#)] [[PubMed](#)]

Disclaimer/Publisher's Note: The statements, opinions and data contained in all publications are solely those of the individual author(s) and contributor(s) and not of MDPI and/or the editor(s). MDPI and/or the editor(s) disclaim responsibility for any injury to people or property resulting from any ideas, methods, instructions or products referred to in the content.